IEEE Open Journal of
Antennas and Propagation

Received XX Month XXXX; revised X Month XXXX; accepted XX Month XXXX. Date of publication XX Month XXXX; date of current version XX Month XXXX.

Digital Object Identifier 10.1109/OAJPE.2020.2976889

A Curved 3D-Printed S-band Patch Antenna for Plastic CubeSat

GIACOMO MUNTONI[1,5], GIORGIO MONTISCI[1,5], SENIOR MEMBER, IEEE, ANDREA MELIS[1], MATTEO BRUNO LODI[1,5], MEMBER, IEEE, NICOLA CURRELI[2], MEMBER, IEEE, MARCO SIMONE[1], GIACOMO TEDESCHI[4], ALESSANDRO FANTI[1,5], SENIOR MEMBER, IEEE, TONINO PISANU[3], ILKA KRIEGEL[2], ATHANASSIA ATHANASSIOU[4], GIUSEPPE MAZZARELLA[1,5], SENIOR MEMBER, IEEE

[1]Department of Electrical and Electronic Engineering, University of Cagliari, 09123 Cagliari, Italy
[2] Functional Nanosystems, Istituto Italiano di Tecnologia, 16163 Genova, Italy
[3]INAF-Osservatorio Astronomico di Cagliari, 09047 Selargius, Italy
[4]Smart Materials, Istituto Italiano di Tecnologia, 16163 Genova, Italy
[5]CNIT , University of Cagliari Research Unit, 09123 Cagliari, Italy
CORRESPONDING AUTHOR: Alessandro Fanti (e-mail: alessandro.fanti@unica.it)

ABSTRACT The new space economy paradigm demands for cost-effective systems for its development. Plastic CubeSats are appealing candidates. To enable the use of this new generation of space systems, the challenge of designing suitable communication sub-systems must be faced. In this work, a 3D-printed ABS antenna easily embeddable in a plastic CubeSat is proposed. The 3D-printed material has been characterized in terms of dielectric, mechanical and thermal properties, and the compliance with space requirements has been assessed. In particular, thermogravimetric and calorimetric tests have been carried out. Static and dynamic mechanical analysis were performed. To comply with the stringent weight and space requirements, the unique antenna design of a curved stacked patch has been proposed. The patch covers the uplink (2.025–2.11 GHz) and downlink (2.2–2.29 GHz) bands for Telemetry Tracking and Command (TT&C) applications, with an overall bandwidth of about 300 MHz (14%). Additionally, taking advantage of the curved shape, the proposed antenna shows a size reduction of the resonant length of about 34%. The size of the antenna is 71.5 x 71.5 x 13 mm^3 and is characterized by a weight of only 51 g . Also, in silico tests, by relying on the measured physical properties and a non-linear numerical model, have been carried out to assess the performances of the final antenna layout during a typical CubeSat mission. The proposed design strategy could be used to develop plastic CubeSats embedding performing antennas.

INDEX TERMS 3D Printing, Antennas, ABS, CubeSats, New Space Economy

I. INTRODUCTION

Conventional satellites, largely employed in space missions over the past decades are characterized by a large mass, which can easily reach 1000 kg, and by a high power consumption [1], [2]. The advent of a brand new compelling space economy, however, calls for a careful choice of cost-effective technologies for future space developments [3]. This trend explains the popularity of the CubeSat standard. CubeSats are compact modular nano-satellites (1–10 kg) that can be realized with commercial off-the-shelf (COTS) components, qualified for spaceflights [2], [4], and whose elementary unit (1U) consists of a cubic module of 10 × 10 × 10 cm^3 size [1], [3]. They are born for educational purposes and soon they came under the spotlight of the space industry for their low cost, lightweight, and low power consumption [5], [6]. These CubeSats features perfectly fit the new space economy paradigm of democratizing the space sector so that innovative systems with short development times (12–18 months) and capable of ensuring a high economic return are needed [7]. In this framework, the cost and weight of these satellites can be further reduced through unconventional development approaches, such as emerging fast-prototyping technologies like 3D printing, if suitable materials are employed. This is why plastic CubeSats have been proposed and investigated [8].

In this respect, few 3D printable plastic filaments have proven to fully comply with the stringent requirements of the CubeSat design specifications, hence can be regarded as available materials for space applications. In particular, one of the main specifications is the low outgassing criterion, according to which CubeSat materials shall have a Total Mass Loss (TML) ≤ 1.0 % and a Collected Volatile Condensable Material

(CVCM) ≤ 0.1 % [9]. The Acrylonitrile Butadiene Styrene (ABS) is a promising material for plastic CubeSats, further lowering their overall cost and mass, being lighter in weight and less expensive than aluminum [8], [10]. It can be proficiently used in vacuum or even high-vacuum environments (e.g., space applications), as shown in [11], where scientists from the National Institute of Standard and Technologies (NIST) reported the outgassing rate of 3D printed ABS in vacuum. The conclusion states that the main gas absorbed by the material from the atmosphere is water and that it can be easily degassed in a relatively short time (3 days at 100 °C). The 3D-printed ABS has been also added by NASA to the list of approved low-outgassing materials, scoring a TML of 0.94 % and a CVCM of 0.04 % [12].

Furthermore, during the 4-year Polymer Erosion and Contamination Experiment (PEACE), wherein 41 different polymers were exposed to the Low Earth Orbit (LEO) environment on the exterior of the International Space Station (ISS) in order to evaluate the atomic oxygen erosion, the ABS stood out for one of the lowest mass losses [13].

Nonetheless, to better understand if the space's harsh environment affects the characteristics of the material, a rigorous thermal and mechanical analysis should be performed. The temperature variation in LEO ranges from -65 °C to 125 °C with thermal cycling depending on the orbit height [14]. However, to mitigate the temperature excursion, satellites employ cooling/heating systems and/or thermal blankets, in such a way that the considered temperature range can be narrowed between -20 °C and 80 °C for most external components (except for solar panels) [10], [15].

In this paper, a thorough analysis of a commercial, transparent 3D plastic filament ABS for CubeSat application is presented. The chosen ABS filament (SUNLU, China) has the peculiar characteristic of being transparent, which opens up the possibility of integrating directly their subsystems, without covering solar panels. The thermal and mechanical properties of 3D printed ABS are retrieved to assess its suitability for a plastic CubeSat. The thermal analysis is particularly useful to evaluate possible changes in the material dielectric permittivity, since the ABS can be used as a substrate for the antennas within the CubeSat communication system, in a convenient integrated system. Indeed, the free-form factor of 3D printing can be exploited to obtain complex shapes, suitable for the CubeSat applications.

As a proof of concept, an S-band curved microstrip patch made of ABS is presented. S-band patch antennas for CubeSat applications are very popular among researchers. Pittella and Nascetti propose a layout based on four rectangular patches on the four sides of a square annular ring, in [15] and [16]. These prototypes are reconfigurable thanks to the changeable phase of the feeding lines. Meshed antennas are proposed in [17] and [18], showing a fully solar-panel integrated circularly polarized patch for CubeSat ground/intersatellite communication [17] and three proximity coupled patches that achieve large bandwidth thanks to the slight difference in size. A dual-band stacked circularly polarized patch antenna is proposed in [19]. Veljovic and Skrivervik design a low-profile antenna, achieving wideband behavior through aperture coupled feeding [20]. A fractal geometry is chosen instead in [21], to obtain a compact, lightweight, and wideband deployable patch antenna. Finally, a dual-fed, dual-circularly polarized antenna fed by 3-dB coupler is presented in [22]. Some of the key parameters of these antennas are reported in Tab. 1.

The proposed antenna is based on the layout of the curved patch proposed in [23], wherein the curvature radius has a notable effect on both fractional bandwidth (which is a product of the increase of the average substrate thickness) and efficiency. In particular, decreasing the curvature radius leads to an increase in bandwidth and efficiency (please refer to Tab. II of [23] for more details). A smaller curvature radius leads also to a gain enhancement, which is contrasted by a reduction of the directivity. This is explained by the reduction of the distance between the radiating edges of the patch, as the curvature radius decreases.

The original layout has been enhanced with a stacked configuration and an additional small air gap within the lower substrate for a further bandwidth and efficiency increment. Furthermore, the curved shape allows for a reduction of the resonant length of the antenna of about 34% w.r.t. its planar counterpart, a desirable feature for CubeSat applications in order to save space for the solar panels [24] and/or other components. The operating bandwidth of the antenna covers both the uplink and downlink bands of the S-band communications frequencies for satellite applications (2.025–2.110 GHz and 2.20–2.29 GHz, respectively). It is characterized by a fractional bandwidth of about 14%, a gain of about 6.7 dBi, high efficiency of 96%, and an overall weight of about 50 g. The size reduction, bandwidth coverage, and lightweight make this antenna particularly appealing for S-band CubeSat applications. With respect to other antennas presented in the literature, the proposed patch is characterized by a novel approach in the prototyping process, relying on the 3D printing, a rather large operating bandwidth, an extremely reduced weight and a very high efficiency. The patch has been designed to fit 1U CubeSats, as shown in Fig. 1, wherein a detailed representation of the antenna integrated in the ABS chassis is reported. However, if needed, the antenna could be also used in a conventional metallic CubeSat, with the printed ABS acting exclusively as substrate for the patch.

It has to be clarified, to avoid any type of confusion that the proposed antenna is not meant to be transparent. One of the authors' intent is to present to the scientific community a suitable 3D printed material for CubeSat applications that has also a degree of transparency, and as such could be employed to design transparent antennas (using meshed configurations or, for example, ITO materials).

TABLE 1. S-band patch antenna comparison table.

Ref.	Size [mm^3]	Center freq. [GHz]	BW [GHz] (%)	Gain [dBi]	Efficiency [%]	Polarization	3D-printed
[15]	96x96x2.1	2.45	0.04 (1.63)	3.7	44.7	LP/CP	No
[16]	96x96x2.1	2.45	0.77 (31.4)	7.3	n/a	CP	No
[17]	40.2x39.5	2.45	0.1 (4)	4.8	n/a	CP	No
[18]	98.8x98.8	2.43	0.064(2.67)	7.2	70	LP	No
[19]	100x100x11	2.2	0.212 (9.66)	5.4	n/a	CP	No
[20]	100x100x12	2.45	0.808 (33)	8	76-90	CP	No
[21]	35x45	2.3	0.66 (28.7)	4.39	n/a	LP	No
[22]	100x100x14.7	2.5	0.28 (11.2)	8.2	n/a	CP	No
This work	71.5x71.5x13	2.16	0.3 (14)	6.7	96	LP	Yes

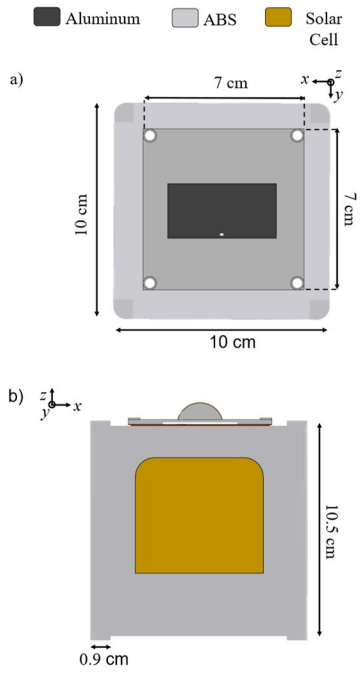

FIGURE 1. Detailed view of the CubeSat architecture with definition of the materials and antenna placement. Top (a) and lateral (b) perspectives of the 1U CubeSat with the plastic stacked patch antenna mounted on the z+-face.

II. ANTENNA DESIGN AND FABRICATION

The presented antenna is composed of two main parts: the bottom layer and the top layer. Fig. 2 shows a dimensional sketch of the bottom layer from the top, front, and side perspectives. This part of the antenna exhibits a layout similar to the rectangular curved patch proposed in [23]. The major differences reside in the substrate material, made, in this case, of Acrylonitrile Butadiene Styrene (ABS, $\varepsilon_r = 2.3$, $\tan\delta = 0.01$ at 2.15 GHz) and in the presence of an air gap encased in the substrate. The latter is an S x S x H_S box (with $S = 71.5$ mm and $H_S = 2.5$ mm) topped by a cylindrical protrusion, made also of ABS, with a bending radius $R_H = 12$ mm. The footprint of the cylindrical protrusion on the x-y plane (see Fig. 2a) has length $W = 50.6$ mm along the x-direction and $L = 23.81$ mm along the y-direction. The bent bottom aluminum patch is placed over the cylindrical protrusion and has a thickness equal to $t_P = 0.050$ mm.

The height of the cylinder above the flat substrate can be simply calculated from the geometrical relationship as $H_B = R_H\,[1 - cos(arcsin\, L/(2R_H))]$ which in this case is equal to 10.5 mm. The feeding is provided through a commercial coaxial connector, placed at distance $y_f = 11.25$ mm from the center of the substrate (see Fig. 2a and 2c), to guarantee the 50 Ω matching. A rectangular W x L_1 x H_A air gap has been placed inside the bottom substrate, in direct contact with the ground plane, wherein $L_1 = 45$ mm, and $H_A = 1$ mm (see Fig. 2). The ground plane is an aluminum plate ($\sigma = 3.5 \cdot 10^7$ S/m) with thickness $t_M = 0.9$ mm. The four holes with diameter $D_H = 5$ mm, placed at the corners of the structure allow a practical sealing through nylon screws and nuts. The holes are surrounded by hollow pillars with diameter $D_P = 7.1$ mm that act as spacers between the two layers, keeping a gap equal to $H_G = 1$ mm. To help the reader, a 3D view of the structure is displayed in Fig. 3a.

In the same fashion, a 3D sketch of the top layer (with a transparent bottom layer) is reported in Fig. 3b. To better understand the overall structure, a cut view of the whole antenna is reported in Fig. 3c as well. With reference to Fig. 3, the top layer substrate has the same thickness as its bottom counterpart. The parasitic aluminum patch (having the same thickness t_P of the bottom one) is also placed over a cylindrical surface characterized by a different bending radius ($R_{H2} = 15.5$ mm) from the same center and by a planar footprint equal to W_2 x L_2 (with $W_2 = 60.6$ mm and $L_2 = 29.33$ mm).

This second cylindrical shape has a height from the top flat substrate equal to $H_{B2} = 10.5$ mm. This means that the overall height of the antenna is 17.4 mm. In order to maintain the chosen gap H_G, the curvature radius of the lower profile of the top layer must be equal to $R_{H3} = R_H + H_G = 13$ mm. A summary of the geometrical parameters of the antenna is reported in the caption of Figs. 2 and 3. It is worth noting that the values of H_A and H_G have been simulated to obtain the best performance in terms of efficiency and to properly cover the S-band uplink and downlink bands.

The substrate of the antenna has been manufactured employing the commercial 3D printer Raise 3D N2 Plus. The details of the printing procedure are summarized in Tab. 2. The height of each extruded layer has been set to 0.1 mm. The thermoplastic filament is a commercial ABS (Sunlu Company). The metallization is provided through aluminum tape for the patches whereas an aluminum plate has been used for the ground. A photo of the realized antenna is shown in Fig. 4. The total weight of the prototype antenna is 51 g,

meaning that this element is extremely lightweight and, thus, well suited for CubeSat applications.

TABLE 2. Printing settings.

Extruding Temperature	Bed Temperature	Nozzle Diameter	Printing Speed
245 °C	50 °C	0.4 mm	55 mm/sec
Retraction Speed	**Layer Height**	**Infill Percentage**	**Infill Pattern**
40 mm/sec	0.1 mm	100%	Rectangular

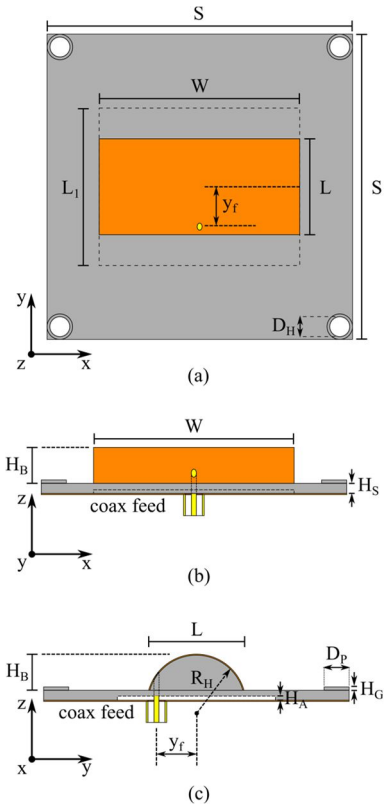

FIGURE 2. Dimensional sketch of the bottom layer of the proposed antenna from top (a), front (b), and side (c) perspectives. Parameter summary: S = 71.5 mm, H_S = 2.5 mm, R_H = 12 mm, W = 50.6 mm, L = 23.81 mm, H_B = 10.5 mm, y_f = 11.25 mm, L_1 = 45 mm, H_A = 1 mm, D_H = 5 mm, D_P = 7.1 mm, H_G = 1 mm.

III. ANTENNA SIMULATIONS AND MEASUREMENTS

The antenna has been designed using CST Studio Suite. After the fabrication, its frequency response, radiation pattern, and gain have been measured in an anechoic chamber using the setup depicted in Fig. 5, which includes the Anritsu MS46322B two-port vector network analyzer (VNA), and a test calibrated antenna (model HyperLOG 7060 by AARONIA AG). The test antenna has been connected to a broadband Low Noise Amplifier (LNA) (model ZX60-83LN-S+ by Minicircuits) to improve the sensitivity of the measurement. The LNA gain has been accurately measured using the VNA to obtain a reliable estimation of the antennas under test gain.

The comparison between simulated and measured $|S_{11}|$ is reported in Fig. 6. It can be noticed the good agreement between the two curves. Concerning the measured S_{11}, the antenna bandwidth is about 300 MHz (14% fractional bandwidth) covering both the S-band TT&C uplink and downlink bandwidths for CubeSat applications. From the CST simulations, it appears that the radiation efficiency of the patch is around 96% over the entire operating bandwidth. The comparison between the measured and simulated gain at room temperature is reported in Fig. 7. The measured gain is about 6.7 dBi in the target bandwidths. Given the measured antenna gain, considering the typical link budget analysis for CubeSat missions [25], the proposed ABS stacked antenna can achieve a signal-to-noise ratio (SNR) of ~11 dB, satisfying the requirement of a 10^{-5} bit error rate for the most common modulations and less than 0.1 dB link margin [26].

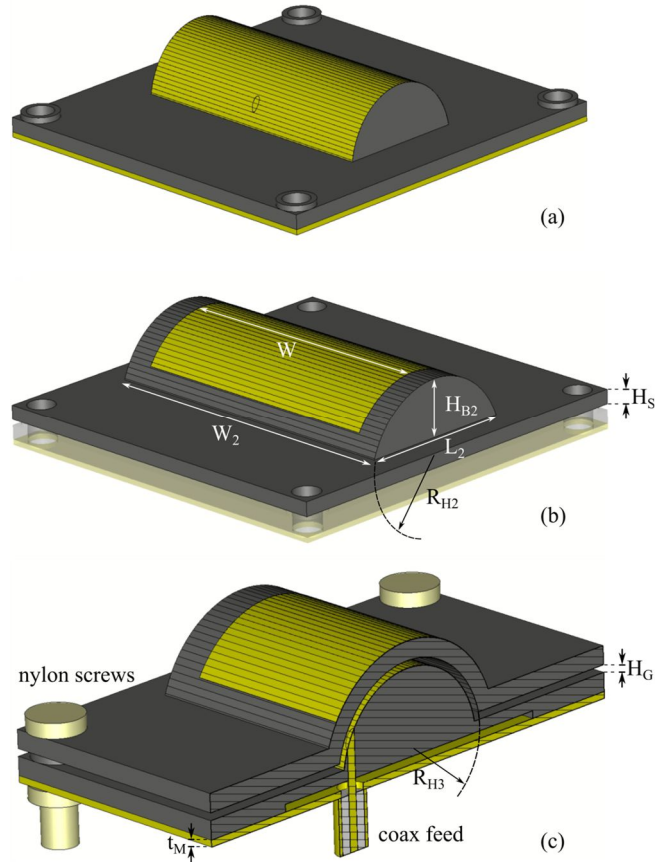

FIGURE 3. 3D view of the proposed antenna: bottom layer (a), top layer (b), and cut view (c). Parameter summary: t_M = 0.9 mm, R_{H2} = 15.5 mm, W_2 = 60.6 mm, L_2 = 29.33 mm, H_{B2} = 10.5 mm, R_{H3} = 13 mm.

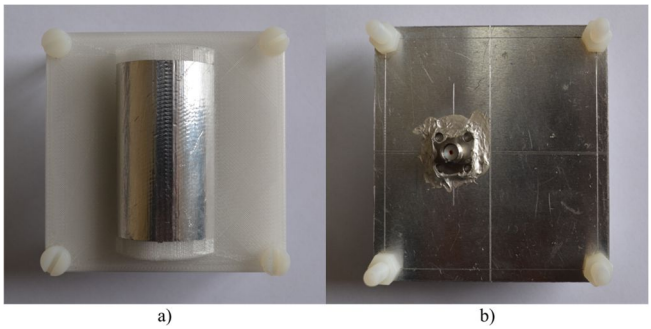

FIGURE 4. **Photo of the realized antenna: front (a), and back (b).**

Finally, the comparison between measured and simulated radiation patterns is reported in Fig. 8, for E-plane e H-plane cuts at 2.16 GHz, showing a good agreement also in this case. The measured radiation patterns are provided only at a central frequency (2.16 GHz) and not at initial (2.025 GHz) of final frequency (2.29 GHz) within the whole operating bandwidth, since there is no substantial difference between the patterns. It is worth noting that the simulated E-plane cross-polar component is not shown because lower than -50 dB. The measured cross-polarization level is around -20 dB, whereas the simulated Front-to-Back (F/B) ratio is about 16. We were not able to measure the back radiation due to the interferences of the test coaxial cable connected to the VNA.

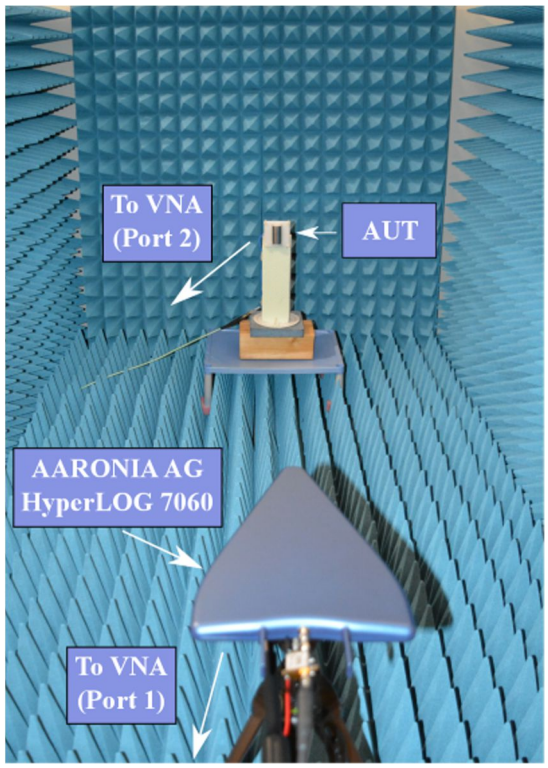

FIGURE 5. **Photo of the measurement setup employed for the S_{11}, radiation pattern, and gain measurements of the prototype antenna.**

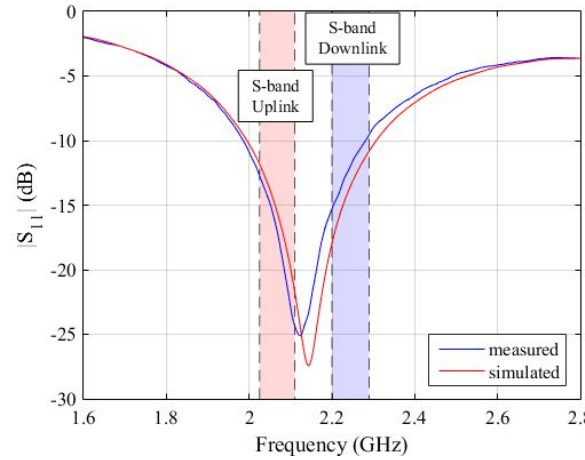

FIGURE 6. **Comparison between measured and simulated $|S_{11}|$ for the proposed antenna.**

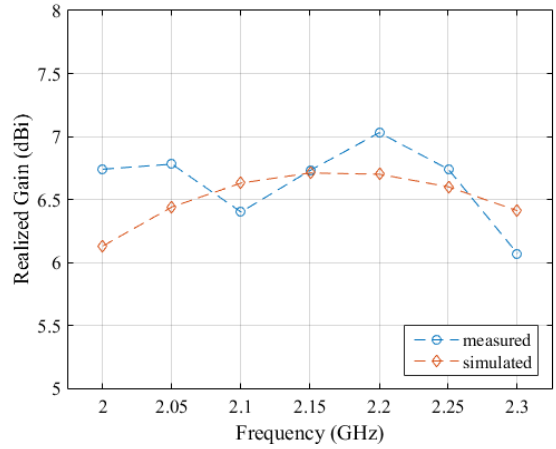

FIGURE 7. **Comparison between measured and simulated gain for the proposed antenna.**

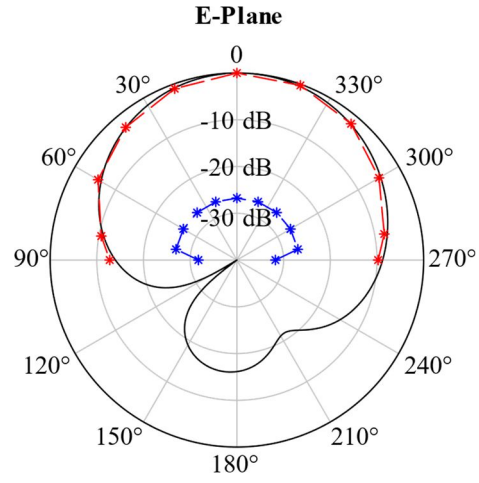

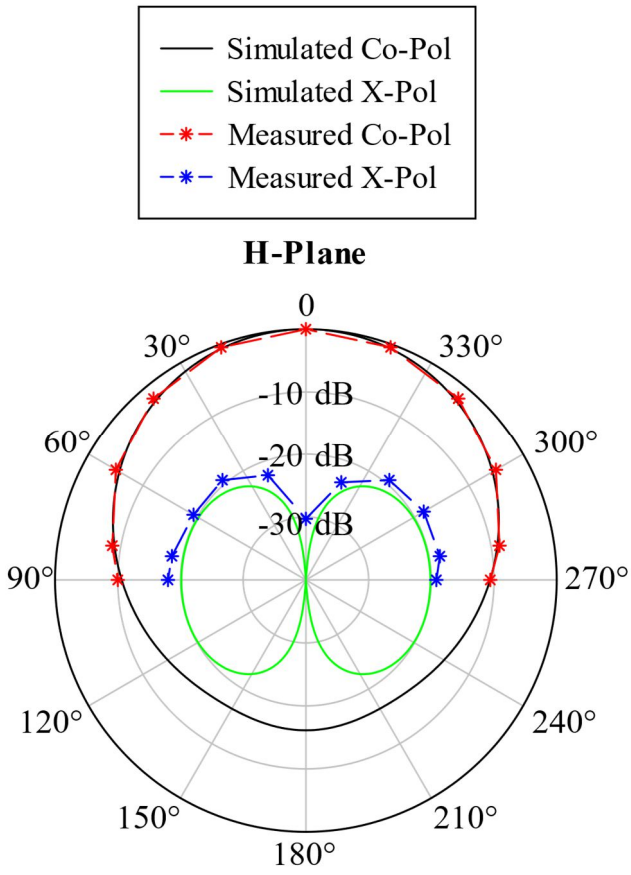

FIGURE 8. Comparison between simulated and measured normalized radiation pattern for E-plane and H-plane cuts. at 2.16 GHz (center band). The simulated cross-polar component for E-plane is not shown because < -50 dB.

IV. MATERIALS AND METHODS

A. DIELECTRIC CHARACTERIZATION OF THE ABS AT DIFFERENT TEMPERATURES

To take into account the temperature influence on the dielectric response of the ABS, a 3 cm cubic sample has been printed using the commercial 3D printer Raise 3D N2 Plus and the dielectric permittivity has been measured using the resonant cavity method [27]. The measurements have been taken with the sample at room temperature, at -20 °C (using cold storage), and at 80 °C (using an oven). The sample temperature has been registered by using a Fluke TiS45 thermographic camera (Fluke Sys., 2% precision, frame rate of 30 Hz).

B. THERMO-MECHANICAL, OPTICAL AND SURFACE ROUGHNESS CHARACTERIZATIONS

The thermal degradation of ABS samples was investigated through thermogravimetric analysis (TGA) using a Q500 analyzer from TA instruments. All measurements were carried out on 3 mg samples in an aluminum pan at a heating rate of 10 °C/min, from 30 to 800 °C in nitrogen atmosphere. The weight loss (TG curve) and its first derivative (DTG curve) were recorded simultaneously as a function of time and temperature.

Differential scanning calorimetry (DSC) thermograms were acquired with a Diamond DSC (Perkin Elmer) from -90 to 250°C for ABS samples under a dry nitrogen flow (50 mL/min) at 10°C/min. A heating-cooling-heating cycle was performed. For this analysis, small pieces (~5 mg) were cut from the films and loaded in hermetic aluminum pans before running the DSC experiment. The melting (T_m) and the glass transition (T_g) temperature were obtained from the second heating cycle.

The mechanical properties of the films were measured by uniaxial tensile test on a dual column Instron 3365 universal testing machine equipped with a 2 kN load cell. Dog-bone-shaped samples (25 mm length, 4 mm width, 2.2 mm thick) were stretched at a rate of 2 mm min^{-1}. All the stress-strain curves were recorded at 25 °C and 44% RH. The tensile measurements were conducted according to ISO 572-2. Seven measurements were carried out for each sample and the results were averaged to obtain a mean value. The Young's modulus, the stress, and the elongation at break values were extracted from the stress-strain curves.

Dynamic mechanical thermal analysis (DMTA) was performed using a TA Instruments DMA Q800 with a dual cantilever clamp. Samples were tested in temperature sweeps from -140 to 160°C with a heating rate of 10°C·min^{-1}. Experiments were performed in a single frequency oscillation mode with a frequency of 10 Hz and a displacement amplitude of 15 µm. The glass transition temperature (T_g) was determined from the loss modulus (E'') peak.

Since the employed printed ABS has transparent characteristics, the authors decided to include an optical characterization as a useful information for the scientific community. This characterization is for dissemination purposes only, as the authors deny any claims for the proposed antenna to be transparent (feature clearly invalidated by the presence of a thick ground plane). The total transmission ($\%T$), reflection ($\%R$), and absorption (Abs) coefficients were derived via a Cary 5000 UV/VIS/NIR spectrophotometer, equipped with an integrating sphere accessory, on a sample with dimension 2 cm x 2 cm x 1 mm. The wavelength range extends from the ultraviolet (300 nm) to the near-infrared (1000 nm) at normal incidence.

Surface roughness was quantified on a Zeta optical profilometer (Zeta Instruments, San Jose, CA, USA); a 20× camera lens was applied.

V. MATERIAL CHARACTERIZATION

Within the temperature range provided in Section IV.A, the permittivity of the ABS sample fluctuated between 2.285 and 2.330. Therefore, we have simulated the designed antenna using the minimum and maximum of this range, founding no

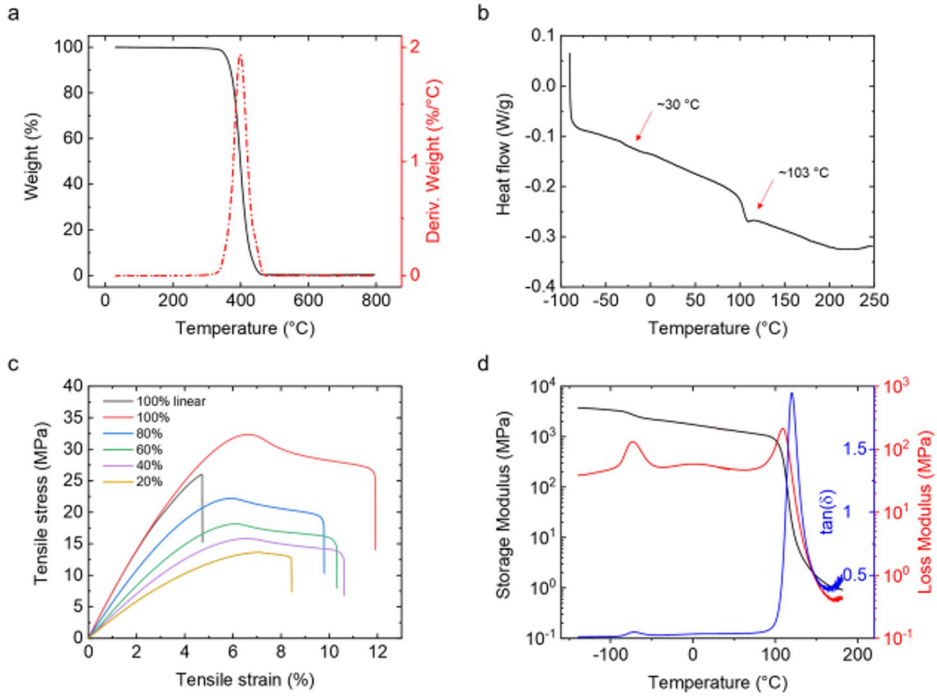

FIGURE 9. **a) Thermogravimetric analysis of ABS sample (black curve). Dashed red curve displays the differential weight. b) DSC analysis of ABS sample, with indication of glass transition temperature. c) Stress-strain curves from tensile test of ABS samples according to the infill percentage. d) Storage Modulus (black curve), Loss Modulus (red curve), and tan(δ_m) (blue curve) from dynamical mechanical analysis of ABS sample with 100% infill percentage.**

variation in the antenna behavior, thus confirming its robustness to space-like thermal excursion, which is a stringent requirement for CubeSat antennas.

The thermal characterization of 3D printed ABS was carried out by thermogravimetric analysis (TGA), shown in Fig. 9a, and differential scanning calorimetry (DSC), displayed in Fig. 9b. From the TGA measurements, ABS resin exhibited a single weight loss at ~400°C corresponding with the structural decomposition of the polymer. A final residue of ~0% was achieved indicating the total combustion of the residual char. The thermal properties of the samples were also characterized by DSC (Fig. 9b). A typical DSC curve for ABS resin was obtained with two major thermal events [28]. The first modest event appears in the range of -50°C to -25°C indicating the rubber-phase glass transition region. The second thermal event takes place from 100°C to 120°C and it is representative of the styrene-acrylonitrile glass transition.

Tensile test and dynamic mechanical analysis (DMA) were used to evaluate the mechanical properties of 3D printed ABS with different percentages of filling (from 20% to 100%). Fig. 9c shows the typical tensile stress-strain curves, while the measured mechanical parameters (*i.e.*, Young's modulus, stress, and strain at break) are reported in Tab.3. It could be observed how the mechanical properties are linearly proportional to the percentage of printing filling. ABS sample with 100% infill interlaced pattern is the sample with the maximum Young's modulus of ~715 MPa, stress at break around ~33 MPa, and good elasticity with ~11% of strain at break. On the contrary, ABS samples with 20% infill interlaced pattern showed a general decrease in the mechanical properties (Young's modulus: ~300 MPa, stress at break: ~14 MPa, strain at break: ~8%). This change can be directly attributed to the different printing fillings which can make the printed sample stronger or weaker when subjected to traction forces. Interestingly, the different infill pattern of ABS filaments from the interlaced to the linear affects the mechanical behavior showing a decrease in the strain at break of ~60% (Fig. 9c). Thermo-mechanical properties were confirmed by DMA (Fig. 9d). In particular, there are no significant differences according to the infill percentage of ABS resin, and two main events can be observed also from this analysis. The first event is a small peak in the tan(δ_m) around -60°C corresponding to the glass transition temperature of the rubbery phase, while the second event in the range of 100 - 130°C is connected to the main glass transition temperature detected also by DSC.

TABLE 3. **Mechanical parameters**

Samples	Young's Modulus (MPa)	Stress at break (MPa)	Strain at break (MPa)
100% lin	714 ± 50	26 ± 2	4.6 ± 0.2
100%	736 ± 5	32 ± 0.6	11 ± 1
80%	578 ± 17	22 ± 0.3	9 ± 0.6
60%	422 ± 17	18 ± 0.1	8.6 ± 1.6
40%	362 ± 15	16 ± 0.2	9.8 ± 1.4
20%	296 ± 22	14 ± 0.3	8.5 ± 0.65
100%	736 ± 5	32 ± 0.6	11 ± 1

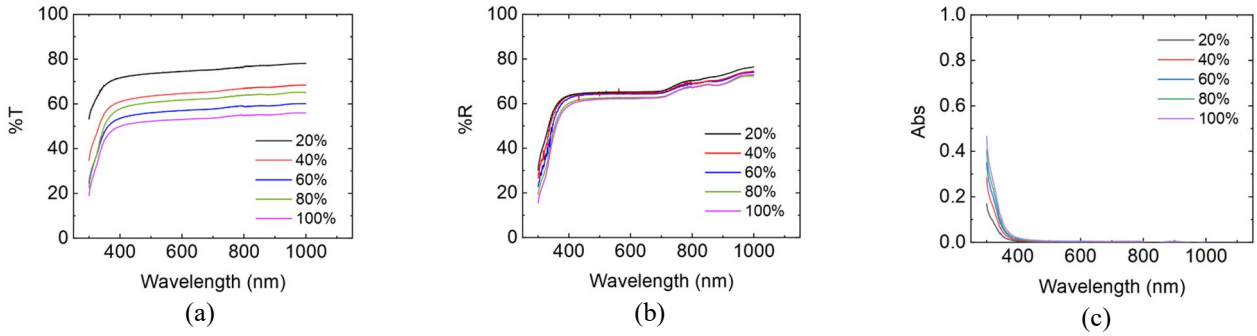

FIGURE 10. **a) Total transmission coefficient (%T) vs. wavelength b) Total reflection coefficient (%R) vs. wavelength. c) Absorption coefficient (Abs), vs. wavelength. The measured optical parameters are given in percentage, from Near UV to Near Infrared.**

The total transmission ($\%T$), reflection ($\%R$), and absorption (Abs) coefficients were derived. The results are shown in Fig. 10 below. It can be noticed that, as the filling factor increases, the transmission decreases to a maximum of about 20%, while decreasing as the wavelength increases. On the other hand, the reflection increases for increasing filling factor, the absorption is higher for higher filling factor, while the difference in the coefficient vanishes above 500 nm. These results highlight that the 100% printed ABS material could be reliably used on CubeSat and does not represent a limiting factor for the solar panels. Indeed, the optical transparency is similar to other materials used found in the literature for similar applications [29], [30]. From the surface roughness analysis, whose results are reported in Fig. 11, we derived that the arithmetical mean height is 0.31 μm, whilst the root mean square height is 0.38 μm. The maximum peak height is 1.35 μm and the deepest pit is 1.19 μm. Considering the working frequency band around 2.1–2.3 GHz, the free-space wavelength is $\lambda_0 \sim 15$ cm and, hence, the roughness of the ABS substrate cannot affect the current distribution on the adhesive copper tape.

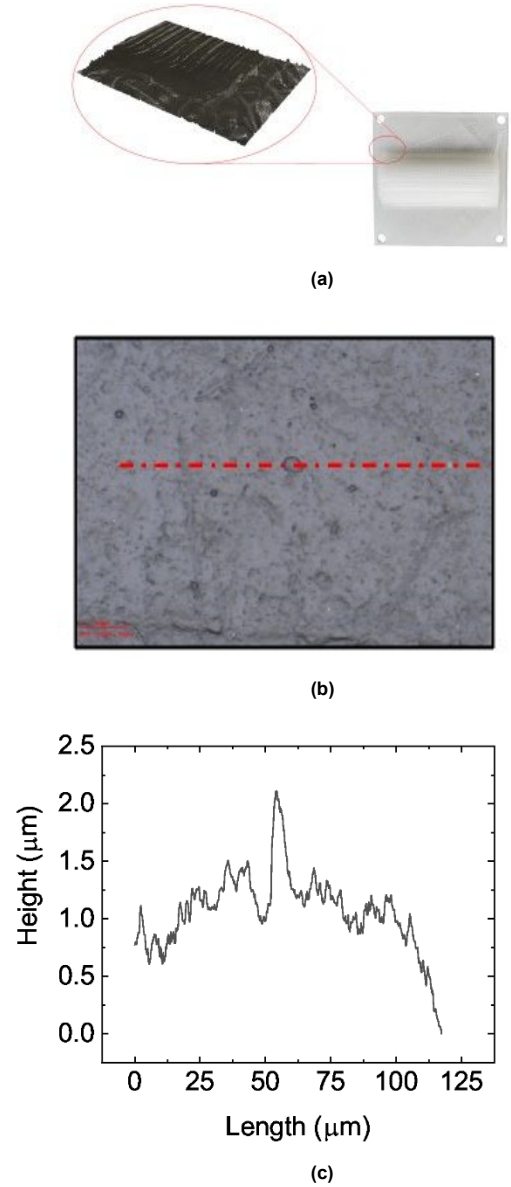

FIGURE 11. **a) Analysis of the surface roughness of the bent patch antenna. b) Scanning line. c) Height profile vs. length, in μm.**

VI. IN SILICO EVALUATION

Given the harsh LEO environment, a coupled mechanical-thermal numerical analysis has been performed to investigate if temperature gradients faced during the orbital cycles can induce mechanical stresses that could potentially lead to antenna damage or failure. Indeed, during the orbit, three main heat sources may drastically affect the operation of the communication device, as shown in Fig. 12a; i.e., the direct sun radiation (Q_s), the albedo radiation (Q_a), and, finally, the infrared energy directly emitted from Earth's atmosphere or surface (Q_e). Considering a LEO mission which consists of a sun-synchronous circular orbit, having an orbital height of 300 km and an orbit inclination angle $\beta = 90°$, the total power fluxes directed on the CubeSat surfaces were computed [31]-[33], and are reported in Fig. 12b. By relying on the multiphysics numerical model reported in [6], we performed simulation by solving the unsteady heat transfer

balance for study the dynamics of the temperature ($T = T(x, y, z, t)$) in the case of a 1U CubeSat, on which the proposed stacked patch antenna is deployed (Fig.1), and derive the deformation and Von Mises stresses (σ_{VM}) distributions using the finite element method (FEM) commercial software Comsol Multiphysics 5.5 (Comsol Inc., MA, US). Homogeneous temperature distribution was assumed as the initial condition, i.e., $T(x, y, z, t = 0) = T_0$. As boundary conditions for the thermal problem, thermal insulation and surface-to-ambient radiation are considered. The external temperature was set to 4 K. The materials properties are reported in Tab. 4. The thermal and mechanical properties of solar cells were taken from [6]. The thermal and mechanical properties of ABS were derived from the experimental characterization. Five orbits, with a 1 min time step, were simulated. The maximum temperature is of ~50°C and it is reached in the top layer of the stacked curved patch antenna (Fig. 13a). On the other hand, the lower antenna layer is colder and can reach a minimum temperature of ~ -100°C, as shown in Fig. 13a.

TABLE 4. Material properties used in the simulations

Property (unit)	Definition	3D-printed ABS	Aluminum
ρ (kg·m^3)	Density	1110	26 ± 2
C_p (J·kg^{-1}K^{-1})	Specific heat	1650	32 ± 0.6
k (W·m^{-1}K^{-1})	Thermal conductivity	0.17	238
α_{ex} (°C^{-1})	Thermal expansion coef.	8.46·10^{-5}	23·10^{-6}
E (MPa)	Young's modulus	736	70·10^3
ν	Poisson's ration	0.36	0.10
η	Emissivity	0.90	0.10

As a matter of fact, the average antenna temperature ranges from ~ -50°C to -100°C and hence the temperature gradients are relatively high (~ 6 °C/cm), as can be seen from Fig. 13a-13c. The thermal stresses induced during the orbits present a narrow range of variation between 6–12 MPa, reaching a maximum of ~ 100 MPa on the antenna edges in the top layer. Probably this is due to the holes presence. The analyzed Von Mises stresses lead to a state of mechanical deformation which deserves to be analyzed to assess if the antenna performances can be degraded.

By analyzing Fig. 13d, it is possible to notice that, after a small transient, the maximum antenna deformation is of ~ 0.38 mm, occurring at the maximum point of cooling (Fig. 13a), and presenting a narrow range of variation (± 0.1 mm/h). We focused on this worst case scenario. On average, the displacement level ranges from 0.1 mm to 0.18 mm. By observing the displacement patterns shown in Fig. 13e and Fig. 13f, a very low retraction around the holes is found (~ 0.35 %), whilst, on the bottom and top layer, the curved patch surfaces, given the air gap below, tends to bend. By simulating the deformed antenna configuration, a difference of ~ 5 dB at the peak of the $|S_{11}|$ response is found. Hence, the antenna performances, i.e., matching and the other radiation properties, are poorly affected by the thermo-mechanical deformation induced by the harsh environment encountered during the orbital periods. It is worth noting that in CubeSat system it is possible to use a temperature control systems and potentially prevent any malfunctioning of plastic antennas [34].

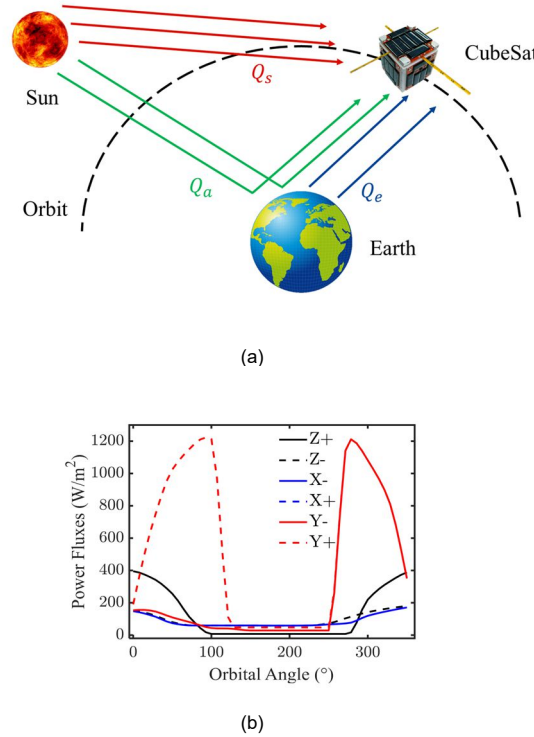

FIGURE 12. a) Schematic description of the thermal conditions in a typical CubeSat mission. b) Power fluxes on the six CubeSat faces (in W/m2) for the case of a typical low earth orbit mission.

VII. CONCLUSION

The paradigm and trend of the new space economy are engaging private stakeholders who demand innovative systems with short development times (12–18 months) and are capable of ensuring a high economic return. In this regard, plastic CubeSat could play a pivotal role in boosting the availability of cost-effective spacecrafts for innovative space missions. Therefore, in this work, a commercial, transparent ABS filament was characterized in terms of dielectric, thermal, and mechanical properties to assess its compliance with space requirements and to retrieve information useful for the design and analysis of a 3D-printed, integrated S-band curved patch antenna. Indeed, some of the most desirable features for a CubeSat antenna include low weight, low cost, wide band, and reduced size to have more space dedicated to the solar panels. In this paper, a curved 3D printed patch

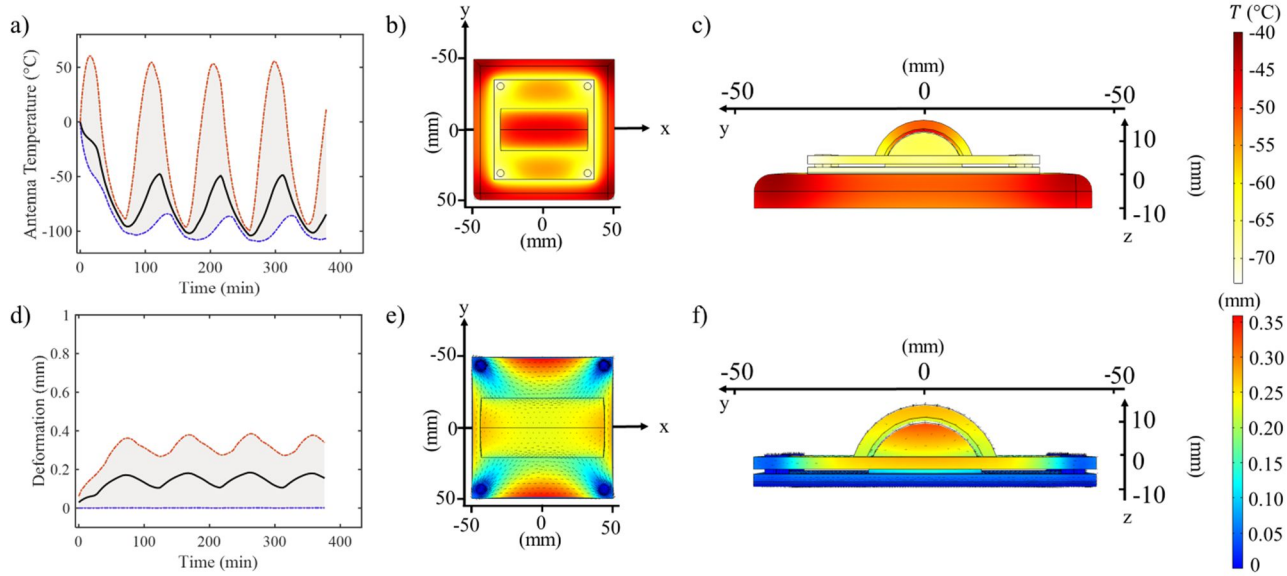

FIGURE 13. **a) Minimum, average and maximum antenna temperature (T(t), in °C). b) Temperature pattern (T(x,y), in °C) for the worst case of maximum deformation. c) Temperature pattern (T(y,z), in °C) for the worst case of maximum deformation. d) Minimum, average and maximum deformation (in mm). e) Displacement field (in mm) on the xy-plane. f) Displacement field (in mm) on the yz-plane.**

antenna capable of meeting all these requirements is presented. The substrate of the antenna is made of ABS, which has proven to be a reliable material for space applications. The proposed antenna covers both the uplink (2.025–2.110 GHz) and downlink (2.2–2.29 GHz) bands of the S-band communications frequencies for satellite applications. It is characterized by a gain of about 6.7 dBi, an efficiency of 96%, a size reduction along the resonant length of about 34% w.r.t. a planar antenna, and most importantly by a total weight of about 50 g, providing a less significant contribution to the total mass of the satellite. Compared with other S-band patch antennas found in the scientific literature, the proposed antenna relies on a fast prototyping process, founded on the 3D printing. Based on the presented study, the viability of plastic CubeSats would enable the possibility to fabricate both the CubeSat chassis and the antenna in a single, convenient, and cost-effective process.

Future works will deal with the re-design and engineering of the proposed antenna layout to develop a fully transparent device, investigating solutions such as meshed patch and ground plane or ITO as conductive material. Moreover, given the innovative character of the proposed antenna concept, its characterization methodology and numerical analysis, this work could be the starting point for studying 3D-printed plastic antennas for large CubeSat units and further advance the flourishing of the new space economy.

ACKNOWLEDGMENT

Nicola Curreli and Ilka Kriegel acknowledge the support of both European Union's Horizon 2020 European Research Council, under grant agreement no. 850875 (I.K.) (Light-DYNAMO), and European Union's Horizon 2020 Research and Innovation program under grant agreement no. 101017821 (I.K.) (LIGHT-CAP).

Alessandro Fanti, Giacomo Muntoni, Matteo Bruno Lodi and Andrea Melis acknowledge the support of the Ministero dello Sviluppo Economico, in AGRIFOOD Programma Operativo Nazionale (PON) Imprese e Competitività (I&C) 2014-2020, through the Project ''Ingegnerizzazione e Automazione del Processo di Produzione Tradizionale del Pane Carasau mediante l'utilizzo di tecnologie IoT (IAPC),'' under Grant CUP: B21B19000640008 COR: 1406652.

The authors would like to thank Dr. Luca Ceseracciu (Material Characterization Facility) and Lara Marini (Smart Materials) for support with mechanical and thermal characterization and the Material Characterization Facility of the Italian Institute of Technology for the access to the equipment.

REFERENCES

[1] H. H. Abdullah, A. Elboushi, A. E. Gohar, and E. A. Abdallah, "An improved S-band CubeSat communication subsystem design and implementation," *IEEE Access*, vol. 9, pp. 45123–45136, Mar. 2021.

[2] S. Habulgasem, F. Tubbal, R. Raad, P. I. Theoharis, S. Lu, and S. Iranmanesh, "Antenna design for CubeSats: a review," *IEEE Access*, vol. 9, pp. 45289–45324, Mar. 2021.

[3] N. Saeed, A. Elzanaty, H. Almorad, H. Dahrouj, T. Y. Al-Naffouri, and M.-S. Alouini, "CubeSat communications: Recent advances and future challenges," *IEEE Commun. Surv. Tut.*, vol. 22, no. 3, pp. 1839–1862, Jul.–Sep. 2020.

[4] F. E. Tubbal, R. Raad, and K.-W. Chin, "A survey and study of planar antennas for pico-satellites," *IEEE Access*, vol. 3, pp. 2590–2612, Dec. 2015.

[5] C. Cappelletti and D. Robson, "CubeSat missions and applications," in CubeSat Handbook. Amsterdam, The Netherlands: Elsevier, 2021, pp. 53–65.

[6] M. Simone, M. B. Lodi, N. Curreli, S. C. Pavone, G. Mazzarella, and A. Fanti, "Optimized design and multiphysics analysis of a Ka-band stacked antenna for CubeSat applications," *IEEE J. Multiscale Multiphysics Comput. Tech.*, vol. 6, pp. 143–157, Sep. 2021.

[7] A. Golkar, A. Salado, "Definition of new space—Expert survey results and key technology trends," *IEEE J Miniaturization Air Space Syst.*, vol. 2, no. 1, pp. 2-9, Mar. 2020.
[8] S. Liu, R. Raad, P. I. Theoharis, and F. Tubbal. "Dual-band folded-end dipole antenna for plastic CubeSats," *IEEE J. Miniaturization Air Space Syst.*, vol. 1, no. 3, pp. 172–178, Dec. 2020.
[9] CubeSat Design Specification Rev. 13," California Polytechnic State University [Online]. Available: https://static1.squarespace.com/static/5418c831e4b0fa4ecac1bacd/t/56e9b62337013b6c063a655a/1458157095454/cds_rev13_final2.pdf.
[10] J. Piattoni, G. P. Candini, G. Pezzi, F. Santoni, and F. Piergentili, "Plastic Cubesat: An innovative and low-cost way to perform applied space research and hands-on education," *Acta Astronautica*, vol. 81, pp. 419–429, Dec. 2012.
[11] M. Sefa, Z. Ahmed, J. A. Fedchak, J. Scherschligt, and N. Klimov, "Gas uptake of 3-D printed Acrylonitrile Butadiene Styrene (ABS) using a vacuum apparatus designed for absorption and desorption studies," *J. Vac. Sci. Technol. A*., vol. 34, no. 6, pp. 1–18, Nov. 2016.
[12] "Outgassing Data for Selecting Spacecraft Materials Online," National Aeronautics and Space Administration [Online]. Available: https://outgassing.nasa.gov/.
[13] K. K. De Groh, B. A. Banks, C. E. McCarthy, R. N. Rucker, L. M. Roberts, and L. A. Berger, "MISS 2 PEACE polymers atomic oxygen erosion experiment on the international space station," *High Perform. Polym.*, vol. 20, pp. 388–409, Jan. 2008.
[14] J. Plante, and B. Lee, "Environmental Conditions for Space Flight Hardware: A Survey," *NTRS-NASA Tech. Rep.*, Jan. 2005. [Online]. Available: https://ntrs.nasa.gov/citations/20060013394.
[15] G. Muntoni, et al. "A curved 3-D printed microstrip patch antenna layout for bandwidth enhancement and size reduction," *IEEE Antennas Wirel. Propag. Lett.*, vol. 19, no. 7, pp. 1118–1122, Jul. 2020.
[16] L. Leszkowska, M. Rzymowski, K. Nyka, and L. Kulas, "High-gain compact circularly polarized X-band superstrate antenna for CubeSat applications," *IEEE Antennas Wirel. Propag. Lett.*, vol. 20, no. 11, pp. 2090–2094, Nov. 2021.
[17] R. G. Carter, "Accuracy of microwave cavity perturbation measurements," *IEEE Trans. Microw. Theory Tech.*, vol. 49, no. 5, pp. 918–923, May 2001.
[18] S. Corpino, M. Caldera, F. Nichele, M. Masoero, and N. Viola, "Thermal design and analysis of a nanosatellite in low Earth orbit," *Acta Astronautica*, vol. 115, pp. 247–261, 2015.
[19] E. M. Filho, L. O. Seman, C. A. Rigo, V. D. P. Nicolau, R. G. Ovejero, V. R. Q. Leithardt, "Irradiation Flux Modelling for Thermal–Electrical Simulation of CubeSats: Orbit, Attitude and Radiation Integration," *Energies*, vol. 13, no. 24, 6691, 2020.
[20] F. Morsch, L. O. S. Edemar, V. D. P. Nicolau, "Simulation of a CubeSat with internal heat transfer using Finite Volume Method," *Applied Thermal Engineering*, vol. 193, 117039, 2021.
[21] H. Blom, R. Yeh, R. Wojnarowski, M. Ling, "Detection of degradation of ABS materials via DSC," *Journal of Thermal Analysis and Calorimetry*, vol. 83, no. 1, pp. 113-115, 2006.
[22] S. Zarbakhsh, et al., "Optically transparent subarray antenna based on solar panel for CubeSat application," *IEEE Transactions on Antennas and Propagation*, vol. 68, no. 1, pp. 319-328, 2019.
[23] R. B. Green, et al., "Optically transparent antennas and filters: A smart city concept to alleviate infrastructure and network capacity challenges," *IEEE Antennas and Propagation Magazine*, vol. 61, no. 3, pp. 37-47, 2019.
[24] O. Popescu, "Power budgets for cubesat radios to support ground communications and inter-satellite links," *IEEE Access*, vol. 5, pp. 12618-12625, 2017.
[25] N. Saeed, A. Elzanaty, H. Almorad, H. Dahrouj, T. Y. Al-Naffouri, M. S. Alouini, "Cubesat communications: Recent advances and future challenges," *IEEE Communications Surveys & Tutorials*, vol. 22, no. 3, pp. 1839-1862, 2020.
[26] S. Corpino, F. Stesina, "Verification of a CubeSat via hardware-in-the-loop simulation," *IEEE Transactions on Aerospace and Electronic Systems*, vol. 50, no. 4, pp. 2807-2818, 2014

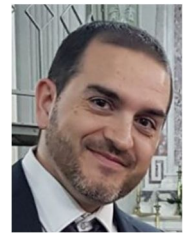

Giacomo Muntoni graduated in Electronic Engineering and Telecommunication Engineering at the University of Cagliari in 2010 and 2015, respectively. In 2019 he received, the PhD in Electronic Engineering and Computer Science, from the University of Cagliari. He is currently working as technologist in the Applied Electromagnetics Group at the University of Cagliari.
His research activity involves: design and characterization of antennas for biomedical and aerospace applications, microwave–based dielectric characterization of materials, 3D printing of RF components, and monitoring of the space debris environment in Low Earth Orbit with the Sardinia Radio Telescope, in collaboration with the Cagliari Astronomical Observatory.

Giorgio Montisci (M'08–SM'19) received the M.S. degree in electronic engineering and the Ph.D. degree in electronic engineering and computer science from the University of Cagliari, Cagliari, Italy, in 1997 and 2000, respectively. Since February 2022, he has been a Full Professor of electromagnetic fields at the University of Cagliari, teaching courses in electromagnetics and microwave engineering. He has authored or coauthored 77 papers in international journals. His current research interests include the analysis and design of waveguide slot arrays, RFID Antennas, wearable antennas, numerical methods in electromagnetics, and microwave circuits and systems. Prof. Montisci is an associate editor of IEEE Access, IET Microwaves, Antennas & Propagation, IET Electronics Letters, and an academic editor of the International Journal of Antennas and Propagation. He was awarded the IEEE Access outstanding Associate Editor of 2020 and 2021.

Andrea Melis received the bachelor's degree in biomedical engineering from the University of Cagliari, Italy, in 2017. He worked as an Assistant Researcher with the University of Cagliari. His research interests include EM modeling and development of RF coils at low and high frequencies, especially for MRI at high field, the design and realization of WSN systems for the monitoring of industrial processes, such as bread manufacturing, and intelligent transportation systems.

Matteo Bruno Lodi (Member, IEEE) received the Bachelor's degree in Biomedical Engineering from the University of Cagliari, Cagliari, in 2016, and the Master's degree in Biomedical Engineering from Politecnico di Torino, Turin, Italy, in 2018. In 2022 he received, with honour, the PhD in Electronic Engineering and Computer Science, from the University of Cagliari. He is currently working as technologist in the Applied Electromagnetics Group at the University of Cagliari. His research activity deals with the modelling of bioelectromagnetic phenomena, especially hyperthermia treatment; the study, manufacturing, and synthesis of magnetic biomaterials for tissue engineering applications; and the use of microwaves for biotechnology and environmental applications, while working in the design and characterization of antennas for space and wearable applications.

He has been awarded as Young Scientists at the General Assembly and Scientific Symposium of URSI in 2020 and 2021. In 2021 he was a co-author of the "2021 IEEE IST Best Student Paper Award" at IEEE International Conference on Imaging Systems & Techniques. He has been appointed as Representative for the Young

Professionals of IEEE Region 8 Nanotechnology Council. He recently joined the NTC technical committee (TC2) Nanobiomedicine, in the frame of the MENED program. He is a member of the Editorial Board of the IEEE Future Directions Technology Policy and Ethics newsletter.

Nicola Curreli (member IEEE) received the M.Sc. degree from the University of Genoa, Genoa, Italy, in 2016, and the Ph.D. degree in Electronic Engineering from the University of Cagliari, Cagliari, Italy, and the Italian Institute of Technology — IIT, Genoa, in 2020. After the Ph.D. degree, he held a fellow position at Graphene Labs — IIT within the WP12 of the Graphene Core 2 Project. In 2019, he was a Visiting Researcher with the Physics and Mechanical Engineering Department, Columbia University, New York City, NY, USA. He is currently a Postdoctoral Researcher at the Functional Nanosystems Group —IIT. His research interests include the study of low-dimensional materials, their characterization, and their application in the field of photonics, as well as the design, implementation, and analysis of linear and nonlinear integrated optical, microwave devices, and antennas. He has been awarded as Young Scientists at the General Assembly and Scientific Symposium of URSI in 2022. He is a member of the Topical Advisory Panel of Photonics.

Marco Simone received the master's degree in electronic engineering and the Ph.D. degree in electronic and computer engineering from the University of Cagliari, Cagliari, Italy, in 2011 and 2016, respectively. He was a Visiting Ph.D. Student with the Queen Mary University of London, London, U.K., in 2015, and a Postdoctoral Research Assistant during 2016–2017 in the same University, with Antennas and Electromagnetics Research Group. Since 2017, he has been an Associate Researcher with the Laboratory of Applied Electromagnetics, University of Cagliari. His research interests include optimization techniques applied to electromagnetics problems, microwave components design for radioastronomy applications, and antennas design.

Giacomo Tedeschi is a Postdoctoral Researcher at the Istituto Italiano di Tecnologia (IIT), in the Smart Materials Group. He has a bachelor degree in Biomedical Engineering from the Università Politecnica delle Marche, Italy (2013) and a MSc in Bioengineering from the Università degli Studi di Genova, Italy (2016). Afterward, he took a PhD in Materials Science and Engineering (2020) from the Università degli Studi di Genova, fully sponsored by Istituto Italiano di Tecnologia (IIT) supervised by Dr. Athanassia Athanassiou and Dr. Josè Alejandro Heredia-Guerrero. He was visiting scientist at the Department of Chemistry and Biochemistry of the City College of New York under the supervision of Prof. Ruth E. Stark. From January 2020 he is involved as Postdoctoral Researcher in R&D industrial/institutional project in Smart Materials Group - IIT on the design and fabrication of sustainable and biodegradable materials able to replace non-biodegradable plastics for specific everyday applications.

Alessandro Fanti (Senior Member, IEEE) received the Laurea degree in electronic engineering and the Ph.D. degree in electronic engineering and computer science from the University of Cagliari, Cagliari, Italy, in 2006 and 2012, respectively. He worked as a Postdoctoral Fellow with the Electromagnetic Group, University of Cagliari, from 2013 to 2016, where he is currently an Assistant Professor. He has coauthored more than 100 scientific contributions published in international journals, conference proceedings, and book chapters. His research interests include the use of numerical techniques for modes computation of guiding structures, optimization techniques, analysis, and design of waveguide slot arrays, analysis, and design of patch antennas, radio propagation in urban environment, modeling of bio-electromagnetic phenomena, and microwave exposure systems for biotechnology and bio-agriculture. He is a member of the IEEE Antennas and Propagation Society, the Italian Society of Electromagnetism, the National Inter-University Consortium for Telecommunications and the Interuniversity Center for the Interaction Between Electromagnetic Fields and Biosystems. Since 2020, he has been acting as a Principal Investigator of the IAPC Project, funded with five million euros by the Italian Ministry of Economic Development (MISE), within the AGRIFOOD PON I&C (2014–2020). He is also an Associate Editor of the IEEE Journal of Electromagnetics, RF and Microwaves in Medicine and Biology.

Tonino Pisanu received the M.S. degree in physics from the University of Cagliari, Cagliari, Italy, in 1995. Since 2001, he has been a Technologist at the National Institute for Astrophysics (INAF), Cagliari Astronomy Observatory, Cagliari. His research interests include analysis and design of microwave components for radio-astronomy applications and in research and development of non-contact measuring systems for characterizing and correcting the optical shape and mechanical configuration of big antenna systems.

Ilka Kriegel started studying nanomaterials during her PhD at the Ludwig-Maximilians-University in Munich, Germany accompanied by a research stay at the University of Chicago, IL, USA. During her first postdoc at the Politecnico di Milano, Italy, she got insight into the ultrafast spectral response of hybrid nanomaterials. A Marie-Curie (global) fellowship brought her to the Molecular Foundry, Berkeley, CA, USA and the Italian Institute of Technology (IIT), Genova, Italy, extending her knowledge to two-dimensional materials. Ilka is now head of the Functional Nanosystems group at IIT holding an ERC Starting Grant (Light-DYNAMO). She is further the coordinator of a collaborative FET Proactive grant (LIGHT-CAP). Her major research interests lie in the exploitation of functional nanosystems for energy and environment. Ilka is mother of three children.

Athanassia Athanassiou is Principal Investigator at the Istituto Italiano di Tecnologia (Genoa, Italy) responsible for the Smart Materials Group. She has a degree in Physics from the University of Ioannina in Greece (1996), an MSc in Laser Photonics from the University of Manchester, UK (1997), and a Ph.D. in Physics, fully sponsored by British Nuclear Fuels Limited (BNFL), from Salford University in Manchester, UK (2000). From 2000, she worked as Post-doc at the Foundation for Research and Technology in Crete, where she became Collaborating Researcher from 2003 until the 2005. In parallel from 2003 to 2005 she was

Academic Staff at the Technical University of Crete, School of Applied Technology. In January 2006, she joint as Researcher the National Nanotechnology Lab, CNR-Istituto di Nanoscienze, Lecce, Italy. In January 2011, she joint the Istituto Italiano di Tecnologia, IIT @ UniLe, Lecce, where she formed the Smart Materials group. The group moved to the central research laboratories of IIT in Genoa in September 2012. In September 2014, she became Tenured, and until now she leads the group of Smart Materials, an interdisciplinary group of about 50 people that deals with the development of sustainable materials and technologies for the benefit of environmental and human health. She has published more than 350 articles in scientific journals, various chapters in scientific books, and has acted as scientific editor. She has 22 Italian and international patents. The last seven years her group has participated in six H2020 EU projects, in
three Institutional projects, in thirty Commercial projects with National and International companies, and has founded two joint labs with industrial partners.

Giuseppe Mazzarella (Senior Member, IEEE) received the degree (summa cum laude) in electronic engineering from the Università Federico II of Naples, in 1984, and the Ph.D. degree in electronic engineering and computer science, in 1989. In 1990, he became an Assistant Professor at the Dipartimento di Ingegneria Elettronica, Università Federico II of Naples. Since 1992, he has been with the Dipartimento di Ingegneria Elettrica ed Elettronica, Università di Cagliari, first as an Associate Professor and then, since 2000, as a Full Professor, teaching courses in electromagnetics, microwave, antennas and remote sensing. He is the author (or coauthor) of over 100 articles in international journals and a reviewer for many EM journals. His research interests include the efficient design of large arrays of slots, power synthesis of array factor, with emphasis on inclusion of constraints, microwave holography techniques for the diagnosis of large reflector antennas, use of evolutionary programming for the solution of inverse problems, in particular problems of synthesis of antennas and periodic structures.